International Symposium
On Turbulence and Shear Flow
Phenomena (TSFP-8)
August 28 - 30, 2013 Poitiers, France

ANALYSIS OF THE EFFECTS OF ROTATION ON AN AXISYMMETRIC WALL JET

Rémi Manceau
Lab. de mathématiques et de leurs applications (LMA)
CNRS–Université de Pau et des pays de l'Adour
IPRA, avenue de l'université
64013 Pau, France
remi.manceau@univ-pau.fr

Rodolphe Perrin
Institut Pprime
CNRS–Université de Poitiers–ENSMA
Bd Marie et Pierre Curie
86962 Futuroscope-Chasseneuil, France
rodolphe.perrin@univ-poitiers.fr

Muhamed Hadžiabdić
Faculty of Engng and Natural Sciences
Intl University of Sarajevo
Paromlinska 66
71000 Sarajevo, Bosnia and Herzegovina
mhadziabdic@ius.edu.ba

Sofiane Benhamadouche
MFEE Department
EDF R&D
6, quai Watier
78401 Chatou, France
sofiane.benhamadouche@edf.fr

ABSTRACT

The case of a turbulent round jet impinging perpendicularly onto a rotating, heated disc is investigated, aiming at understanding the mechanisms at the origin of the influence of rotation on the radial wall jet and associated heat transfer. The present study is based on the complementary use of an analysis of the order of magnitudes of the terms of the mean momentum and Reynolds stress transport equations, available experiments and dedicated Reynolds-Averaged Navier–Stokes (RANS) computations with refined turbulence models. The analysis identifies a scenario for the appearance of rotational effects when the rotation rate is gradually increased.

INTRODUCTION

The case of a jet impinging on a rotating disk, relevant to cooling processes in many industrial applications, implies a complex interaction between the radial wall jet and the azimuthal boundary layer, as shown in Fig. 1. The present collaborative work was initiated in the frame of the workshop organized at TU Graz, Austria, under the auspices of the Special Interest Group 15 *turbulence modelling* of ERCOFTAC (Steiner *et al.*, 2009), and provides an example of cross-fertilization of analytical, experimental and numerical studies. The configuration, based on flow field and heat transfer measurements performed by Minagawa & Obi (2004) and Popiel & Boguslawski (1986), respectively, is issuing with the bulk velocity U_j from a pipe of diameter D ($Re_j = U_j D/\nu = 14{,}500$), at $H = 5D$ from a rotating disk of diameter $R = 6D$. Several rotation rates are investigated, $\omega D/U_j = 0$, 0.12, 0.24 and 0.48.

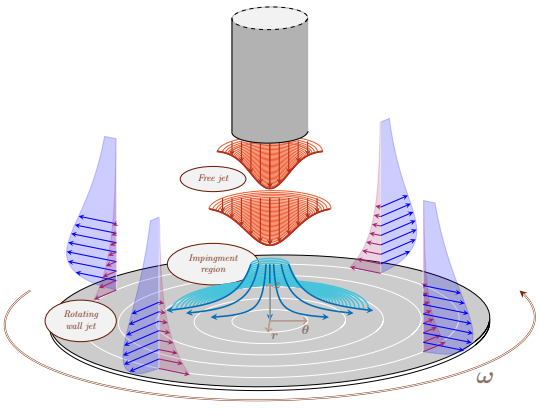

Figure 1. Artist view of the different regions of the flow.

The computations were performed using two in-house codes, T-FlowS (Ničeno & Hanjalić, 2004) developed at Delft University of Technology and the open-source (www.code-saturne.org) *Code_Saturne* developed at EDF (Archambeau *et al.*, 2004). As usual in the ERCOFTAC SIG-15 workshop series, the groups computed the cases independently and performed grid refinement studies. The ζ–f model (Hanjalić *et al.*, 2004) was used in T-FlowS (International university of Sarajevo); the k–ω–SST (Menter, 1994) and φ–f (Hanjalić *et al.*, 2005) models were used in *Code_Saturne* (EDF); the Elliptic-Blending Reynolds stress model (EB-RSM, Manceau & Hanjalić, 2002) was also used in *Code_Saturne* (Institute Pprime/LMA). As concerns heat transfer modeling, the eddy-viscosity models were associated with the SGDH, while the Reynolds stress models were associated with the GGDH.

The rms radial velocities for cases without and with rotation are shown in Fig. 2. The models have difficulties to reproduce the impingement region, a behaviour analyzed in detail in a previous paper (Manceau *et al.*, 2009), mainly linked to the overestimation of the spreading of the free jet before impingement. The present paper focuses on the radial wall jet, i.e., the region $r/D > 2.5$.

Ouside of the region $r/D < 2.5$, dominated by pressure and convection terms, the influence of rotation increases

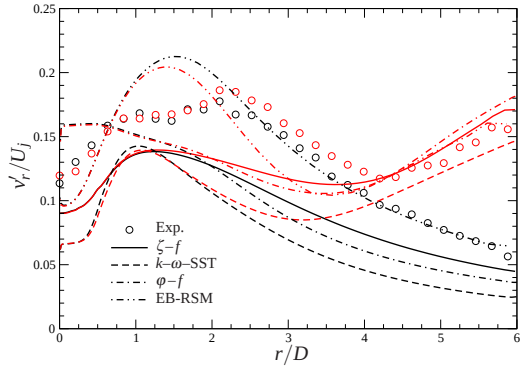

Figure 2. Profiles of the rms radial velocity at $z/D = 0.032$. Black: no rotation; Red: $\omega D/U_j = 0.48$.

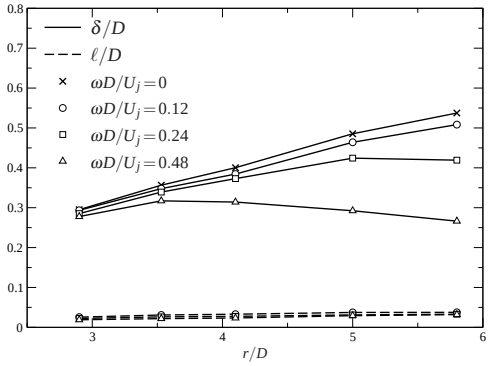

Figure 3. Thicknesses of the wall jet and the azimuthal boundary layer (EB-RSM).

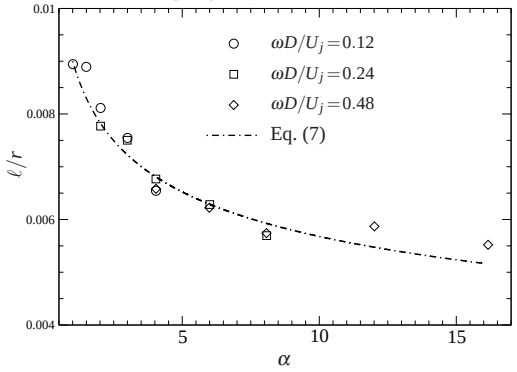

Figure 4. Influence of rotation on ℓ/r (EB-RSM).

with the rotation rate and the distance to the symmetry axis (Fig. 2). The modification of $\partial V_r/\partial z$ due to both the acceleration and the thinning of the wall jet implies an increase of turbulent production, which generates strong radial fluctuations v'_r. Such an effect is captured by all the models, but eddy-viscosity models give a much too early ($r/D \approx 2$ rather than $r/D \approx 4$) increase of v'_r, which shows that this intermediate region is more difficult to reproduce.

The present paper aims at extending the limited knowledge and understanding of this case, in particular as concerns the mechanisms of the migration from a self-similar axisymmetric solution to a rotation-dominated flow.

STRUCTURE OF THE WALL JET

In the absence of rotation, the wall jet can be characterized by the maximum velocity $V_{r\max}$ and the thickness δ

$$\delta = \frac{1}{V_{r\max}} \int_0^\infty V_r(z)\mathrm{d}z. \qquad (1)$$

Due to entrainment, the flow rate $Q(r)$ across the surface at a fixed r is larger than the flow rate issuing from the pipe $Q_j = \pi \frac{D^2}{4} U_j$, and the *entrainment ratio* is defined as $e = Q(r)/Q_j$. A *reduced thickness* $\delta' = 8\delta/e$ is introduced, such that

$$V_{r\max} = \frac{U_j D^2}{r\delta'} \ . \qquad (2)$$

The wall jet can be considered a two-layer flow: the region located between the wall and $\delta_{r\max}$ (location of the velocity maximum), called the inner region, exhibits characteristics close to those of a boundary layer; the region beyond $\delta_{r\max}$, called the outer region, is similar to a free shear flow, and is governed by inviscid equations.

The standard definition of a scale of change in the r-direction, L, used for plane flows, $\partial U/\partial x \sim U_{\max}/L$ (where $\sim$ stands for *of the order of magnitude of*), is replaced by

$$\frac{1}{r}\frac{\partial r V_r}{\partial r} \sim \frac{V_{r\max}}{L} \quad \text{where} \quad \frac{1}{L} = \frac{1}{\delta'}\frac{\partial \delta'}{\partial r} \ . \qquad (3)$$

The standard analysis of this nearly parallel flow shows that the radial wall jet satisfies standard boundary layer equations, which admit a self-similar solution with power-law evolutions of δ, δ' and e in the radial direction, and a linear growth of L, and, consequently, power law evolutions of both $V_{r\max}$ and $\Delta T = T_w - T_\infty$.

Finally, the reduced thickness δ'/D exhibits a very slow variation in the radial direction, and can be, for order of magnitude evaluations below, considered a constant and close to unity. Consequently, Eq. (2) leads to

$$\frac{V_{r\max}}{U_j} \approx \left(\frac{r}{D}\right)^{-1} \ . \qquad (4)$$

As suggested by Glauert (1956), the inner layer can be described using Kármán's method, such that the friction coefficient and the Nusselt number can be shown to behave as

$$C_f = \frac{\tau_w}{\frac{1}{2}\rho U_j^2} = \frac{V_{r\max}^2}{U_j^2}\frac{\tau_w}{\frac{1}{2}\rho V_{r\max}^2} \propto \frac{1}{Re_j^{1/4}}\left(\frac{r}{D}\right)^{-1.95} \qquad (5)$$

$$\text{and} \quad Nu = \frac{\dot{q}_w D}{(\lambda \Delta T)} \propto Re_j^{3/4}\left(\frac{r}{D}\right)^{-1} \ . \qquad (6)$$

INFLUENCE OF ROTATION

In the case of the boundary layer developing on a rotating disk in a quiescent environment, it can be shown (e.g., Dorfman, 1963) that the thickness ℓ of the boundary layer scales with the local Reynolds number $Re_r = r^2\omega/\nu$

$$\frac{\ell}{r} \propto \left(\frac{r^2\omega}{\nu}\right)^{-\frac{1}{5}} = \alpha^{-\frac{1}{5}} Re_j^{-\frac{1}{5}} \ \text{where} \ \alpha = \frac{r^2\omega}{U_j D} \qquad (7)$$

For weak rotation rates, rotation only moderately affects the thickness δ of the wall jet (see Fig. 3) and Fig. 4

shows that the thickness of the azimuthal boundary layer satisfies Eq. (7). Thus, their ratio

$$\frac{\ell}{\delta} \propto \left(\frac{r^2\omega}{\nu}\right)^{-1/5} = \alpha^{-1/5} Re_j^{-1/5} \left(\frac{r}{D}\right)^{0.2} \qquad (8)$$

is small, owing to the high Reynolds number, as can be seen in Fig. 3, where $\ell = \frac{1}{r\omega}\int_0^\infty V_\theta dz$. Since ℓ decreases with the rotation rate, the increasing influence of rotation on the outer layer of the wall jet cannot be attributed to a growing of ℓ, but rather to an interaction between the rotation-induced boundary layer and the inner layer of the wall jet, which modifies the equilibrium between the inner and outer layers.

Limit of strong rotations

In the inner layer, centrifugal acceleration becomes dominant in the radial momentum equation in the limit $\omega \to \infty$, leading to

$$\underbrace{V_r \frac{\partial V_r}{\partial r}}_{\sim \frac{V_r^2}{r}} - \underbrace{\frac{V_\theta^2}{r}}_{\sim r\omega^2} = 0, \qquad (9)$$

which yields $V_r \sim r\omega$. The primary effect of rotation is thus an acceleration of the inner layer. Although the centrifugal acceleration does not directly affect the outer layer, the acceleration of the inner layer necessarily leads to a suction of fluid at the bottom of the outer layer, by mass conservation, such that V_r in the outer layer also scales as $V_r \sim V_{r_{\max}} \sim r\omega$.

Since $rV_{r_{\max}}$ is constant in the absence of rotation, the influence of rotation is characterized by

$$\frac{rV_{r_{\max}}}{(rV_{r_{\max}})_0} \sim \frac{rV_{r_{\max}}}{U_j D} \sim \alpha\,, \qquad (10)$$

where the index $_0$ denotes the non-rotational case. Since Eq. (2) is exact, this result is equivalent to

$$\frac{\delta'}{\delta'_0} \sim \frac{1}{\alpha}\,, \qquad (11)$$

showing a thinning of the wall jet. Fig. 5 confirms the scaling laws (10) and (11), even though discrepancies are observed in the slopes predicted by the different models.

For large α's, the dynamics is dominated by centrifugal acceleration, and the influence of the turbulence model is weak. Therefore, as can be seen in Fig. 2, reproducing the effects of rotation is more challenging for turbulence models in the region located between the impingement region and the rotation-dominated region, and for intermediate rotation rates.

It is confirmed by Fig. 7, for both experiments and EB-RSM results, that the rotation of the disk does not directly affect the turbulence in the outer layer (down to $z/D \approx 0.3$). Consequently, as can be seen in Fig. 9, the entrainment ratio is independent of the rotation rate. The situation is different for eddy-viscosity models, because the turbulent shear

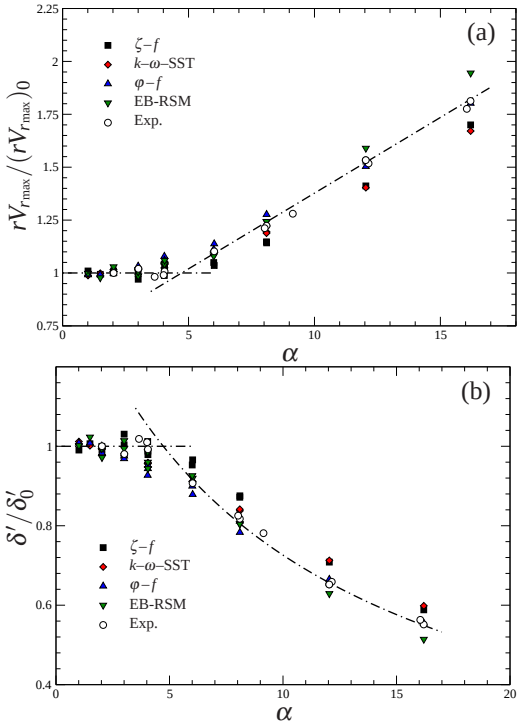

Figure 5. Scaling with α of (a) $rV_{r_{\max}}/(rV_{r_{\max}})_0$ and (b) δ'/δ'_0. Lines: theoretical relations fitted to the experimental results.

stress is assumed proportional to the mean shear, which is modified by the acceleration and thinning of the wall jet.

Since the thickness δ of the jet is related to the entrainment ratio e and the reduced thickness δ' by $\delta = e\delta'/8$, and e is independent of the rotation rate, we have also $\delta/\delta_0 \sim \alpha^{-1}$. Fig. 6a confirms this scaling for strong rotation rates ($\alpha > 5$). Minagawa & Obi (2004) conjectured this scaling, but, due to limitations inherent to the experimental approach, they monitored the variation of the location of the velocity maximum, $\delta_{r_{\max}}/\delta_{r_{\max}0}$. As shown in Fig. 6b, this quantity does not scale very well with α^{-1}, contrary to δ.

Fig. 8 shows the evolution of the Nusselt number based on the radial location $Nu_r = hr/\lambda$ as a function of the rotational Reynolds number $Re_r = \omega r^2/\nu = \alpha Re_j$. It can be observed that the results of the ζ–f and k–ω–SST models well satisfy the scaling proposed by Popiel & Boguslawski (1986), $Nu_r = f(Re_r)$, contrary to the φ–f model that shows some scatter, due to the lack of self-similarity of the solution. For high values of Re_r, it is expected that the Nusselt number approaches the asymptote $Nu_r \propto Re_r^{0.8}$ applicable to a rotating disk in still air (Dorfman, 1963). It can be seen that the present computations, for all the models, seems to approach the correct asymptotic behavior.

Appearance of rotational effects

Momentum equation As long as the rotation rate is sufficiently weak, the self-similar solution for the outer layer holds, and the description of the inner layer given above is valid. In the inner layer, the scales are u_τ and ν/u_τ, where u_τ can be obtained from Eq. (5),

$$u_\tau \sim \frac{1}{Re_j^{1/8}} \frac{U_j D}{r} \left(\frac{r}{D}\right)^{0.025} \sim \frac{1}{Re_j^{1/8}} \frac{U_j D}{r}\,. \qquad (12)$$

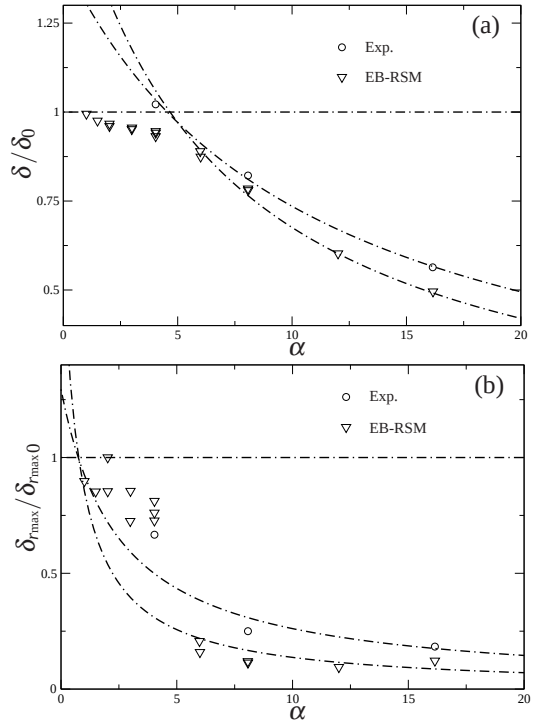

Figure 6. Scaling with α of (a) δ/δ_0 and (b) $\delta_{r\max}/\delta_{r\max 0}$. Lines: theoretical relations fitted to the experimental and numerical results.

The factor $(r/D)^{0.025}$ is ignored in this relation since its order of magnitude is unity.

Since the azimuthal velocity is $V_\theta \sim r\omega$, the radial momentum equation reads, at leading order,

$$\underbrace{-\frac{V_\theta^2}{r}}_{\sim r\omega^2} = \underbrace{\nu\frac{\partial^2 V_r}{\partial z^2}}_{\sim Re_j^{5/8}\frac{U_j^2D^2}{r^3}} - \underbrace{\frac{\partial \overline{v_r v_z}}{\partial z}}_{\sim Re_j^{5/8}\frac{U_j^2D^2}{r^3}} \tag{13}$$

Consequently, the relative weight of the centrifugal acceleration in this equation is

$$\frac{r^4\omega^2}{Re_j^{5/8}U_j^2D^2} = \frac{\alpha^2}{Re_j^{5/8}}, \tag{14}$$

such that the centrifugal acceleration remains negligible for $\alpha \ll Re_j^{5/16}$. Figs. 5 and 6 show a transition in the region $\alpha \approx 5$, which suggests the threshold $\alpha \approx 0.25\,Re_j^{5/16}$.

Production terms For the non-rotating case, the components of the production tensor reduce to

$$\begin{aligned}
P_{rr} &= P_{rr}^{(1)} + P_{rr}^{(2)} = -2\overline{v_r^2}\frac{\partial V_r}{\partial r} - \underline{2\overline{v_r v_z}\frac{\partial V_r}{\partial z}} \\
P_{\theta\theta} &= P_{\theta\theta}^{(1)} = -2\overline{v_\theta^2}\frac{V_r}{r} \\
P_{zz} &= P_{zz}^{(1)} + P_{zz}^{(2)} = -2\overline{v_r v_z}\frac{\partial V_z}{\partial r} - \underline{2\overline{v_z^2}\frac{\partial V_z}{\partial z}} \\
P_{rz} &= P_{rz}^{(1)} + P_{rz}^{(2)} + P_{rz}^{(3)} = -\overline{v_r^2}\frac{\partial V_z}{\partial r} + \overline{v_r v_z}\frac{V_r}{r} - \underline{\overline{v_z^2}\frac{\partial V_r}{\partial z}} \\
P_{r\theta} &= P_{\theta z} = 0
\end{aligned} \tag{15}$$

(the underlined terms are those related to $\partial V_r/\partial z$ and are dominant). When the disk is rotated, additional terms appear,

$$\begin{aligned}
P_{rr}^{(r)} &= 2\overline{v_r v_\theta}\frac{V_\theta}{r} \\
P_{\theta\theta}^{(r)} &= P_{\theta\theta}^{(r1)} + P_{\theta\theta}^{(r2)} = -2\overline{v_r v_\theta}\frac{\partial V_\theta}{\partial r} - 2\overline{v_\theta v_z}\frac{\partial V_\theta}{\partial z} \\
P_{r\theta}^{(r)} &= P_{r\theta}^{(r1)} + P_{r\theta}^{(r2)} + P_{r\theta}^{(r3)} + P_{r\theta}^{(r4)} + P_{r\theta}^{(r5)} \\
&= -\overline{v_r^2}\frac{\partial V_\theta}{\partial r} + \overline{v_r v_\theta}\frac{\partial V_z}{\partial z} - \overline{v_r v_z}\frac{\partial V_\theta}{\partial z} + \overline{v_\theta^2}\frac{V_\theta}{r} - \overline{v_\theta v_z}\frac{\partial V_r}{\partial z} \\
P_{\theta z}^{(r)} &= P_{\theta z}^{(r1)} + P_{\theta z}^{(r2)} + P_{\theta z}^{(r3)} + P_{\theta z}^{(r4)} \\
&= -\overline{v_r v_\theta}\frac{\partial V_z}{\partial r} + \overline{v_\theta v_z}\frac{\partial V_r}{\partial r} - \overline{v_r v_z}\frac{\partial V_\theta}{\partial r} - \overline{v_z^2}\frac{\partial V_\theta}{\partial z}, \\
P_{rz}^{(r)} &= \overline{v_\theta v_z}\frac{V_\theta}{r}
\end{aligned} \tag{16}$$

Some of the production terms, evaluated from the EB-RSM computations, are plotted in Fig. 11, at the edge of the disk. The orders of magnitude of the different terms can be readily deduced from previous sections, and depend on the region of the flow.

Outer layer Since we have shown that the outer layer is not directly affected by the azimuthal boundary layer, the production tensor in the outer layer must keep the same structure as in the case without rotation, and the following orders of magnitude are obtained

$$P_{rr} \sim P \sim u^2\frac{V_{r\max}}{\delta}; \quad P_{\theta\theta} \ll P; \quad P_{zz} \ll P; \quad P_{rz} \sim P \tag{17}$$

where the $P \sim \frac{1}{2}P_{rr}$ is the kinetic energy production. In the outer region, approximately located between $z/D = 0.1$ and $z/D = 1$ (Fig. 11), production is dominated by $P_{rr}^{(2)}$ (due to $\partial V_r/\partial z$). Terms $P_{rr}^{(1)}$, $P_{\theta\theta}^{(1)}$, $P_{zz}^{(1)}$ and $P_{zz}^{(2)}$, related to the radial expansion of the jet, are lower at least by a factor of δ/r.

Fig. 11 shows that in the outer layer, this description of the production tensor remains valid for all the rotation rates, which confirms that the outer layer is not directly affected by the rotation-induced boundary layer. The production terms are however increased as a consequence of the modification of the velocity gradient $\partial V_r/\partial z$.

Consequently, the budgets of the Reynolds stresses (Fig. 12) are very similar to the case of a standard boundary layer, even when the disk rotates: the velocity gradient $\partial V_r/\partial z$ induces turbulent production on the longitudinal component (here, $\overline{v_r v_r}$), and energy is then redistributed to other components via the pressure term. However, due to the radial expansion of the jet, convection is active and $P_{\theta\theta}$ and P_{zz} are not zero.

Inner layer In this region, located between the wall and $z/D \approx 0.1$ (Fig. 11a0), scales are u_τ and ν/u_τ, with u_τ given by Eq. (12), such that we have

$$P_{rr} \sim Re_j^{1/2}\frac{U_j^3D^3}{r^4}; \quad P_{\theta\theta} \ll P; \quad P_{zz} \ll P; \quad P_{rz} \sim P \tag{18}$$

Contrary to the outer layer, additional terms appear in the production tensor (Fig. 11), and, aiming at identifying a

threshold, the analysis below considers the introduction in the equations of a gradually increasing rotation rate.

A straightforward, albeit long, analysis provides the following evaluations for the production terms due to rotation:

$$\begin{aligned} P_{rr}^{(r)} &\sim P_{rz}^{(r)} \sim \frac{\alpha^2}{Re_j^{3/4}} \frac{U_j D}{r\ell} u_\tau^2 \\ P_{\theta\theta}^{(r)} &\sim \frac{\alpha^2}{Re_j^{3/4}} \frac{U_j D}{\ell^2} u_\tau^2 \\ P_{r\theta}^{(r)} &\sim P_{\theta z}^{(r)} \sim \alpha \frac{U_j D}{r\ell} u_\tau^2 \,. \end{aligned} \tag{19}$$

As long as α is sufficiently weak, the production terms due to rotation are negligible compared to those already present in the non-rotating case except for $P_{r\theta}^{(r)}$ and $P_{\theta z}^{(r)}$, since $P_{r\theta} = P_{\theta z} = 0$.

When α is increased, the main effect is the rapid increase of $P_{\theta\theta}^{(r2)}$. Since, in the absence of rotation, the production term $P_{\theta\theta}$ is small compared to P (and negative), $\overline{v_\theta^2}$ essentially receives energy from other terms (redistribution, convection, diffusion), and these terms are of the same order of magnitude as production P. The correct criterion to evaluate the influence of rotation on $\overline{v_\theta^2}$ is then the ratio

$$P_{\theta\theta}^{(r)}/P \sim \alpha^{12/5} Re_j^{-11/10} \,. \tag{20}$$

It can be seen in Fig. 11a1 and b1 that, when rotation is increased, the term $P_{\theta\theta}^{(r2)}$ rapidly becomes much stronger than P_{rr}, such that the turbulence anisotropy is completely modified and, as can be seen in Fig. 12, energy transfer mechanisms are reversed (production of $\overline{v_\theta^2}$ and redistribution towards other components). The order of magnitude analysis leading to Eq. (20) thus shows that the value of α for which $P_{\theta\theta}^{(r2)}$ becomes significant scales with $Re_j^{11/24}$, but a closer inspection of the level of $P_{\theta\theta}^{(r2)}$ as a function of α in our numerical results suggests that the threshold is about $\alpha \approx 0.01 Re_j^{11/24}$. To say the obvious, such effects of rotation on turbulence cannot be reproduced by linear eddy-viscosity models, which are completely insensitive to rotation: they only reproduce the increase of $\overline{v_\theta^2}$ with rotation that results from the increase of V_r due to the centrifugal acceleration.

CONCLUSIONS

The order of magnitude analysis supports a scenario for the gradual increase of the influence of rotation. For low rotation rates, such that $\alpha < 0.01 Re_j^{11/24}$, the flow is in a *superposition regime* (see Fig. 10), in which the rotation-induced boundary layer does not significantly affect the self-similar wall jet. For intermediate rotation rates, $0.01 Re_j^{11/24} < \alpha < 0.25 Re_j^{5/16}$, an *interaction regime* is observed, in which the inner layer resemble an Ekman layer, while the outer layer remains weakly perturbed. Finally, for strong rotation rates, $\alpha > 0.25 Re_j^{5/16}$, in the *rotation-dominated* regime, centrifugal acceleration becomes dominant and causes an intensification and thinning of the jet.

Therefore, depending on the value of the parameters α and Re_j, the modification of the wall jet can be linked to the influence of the centrifugal acceleration, or to more complex effects due to the anisotropic transfer of energy from the mean flow to the turbulent field. The linear eddy-viscosity models are able to reproduce the former effects, in the rotation-dominated regime: acceleration and thinning of the jet (independent of turbulence modeling); intensification of the shear, and consequently of turbulence production. The more complex effects appearing in the interaction regime, when the skewing of the inner layer of the wall jet completely modifies the structure of the different terms in the Reynolds stress budgets, require the use of a more elaborate model.

REFERENCES

Archambeau, F., Méchitoua, N. & Sakiz, M. 2004 Code Saturne: A Finite Volume Code for the Computation of Turbulent Incompressible flows - Industrial Applications. *Int. J. on Finite Volume, Electronical edition: http://averoes.math.univ-paris13.fr/html* **ISSN 1634** (0655).

Dorfman, L. A. 1963 *Hydrodynamic resistance and the heat loss of rotating solids*. Oliver & Boyd, Edinburgh-London.

Glauert, M.B. 1956 The wall jet. *J. Fluid Mech.* **1** (6), 625–643.

Hanjalić, K., Laurence, D. R., Popovac, M. & Uribe, J. C. 2005 $(\overline{v^2}/k)$–f turbulence model and its application to forced and natural convection. In *Proc. 6th ERCOFTAC Int. Symp. on Eng. Turb. Modelling and Measurements, Sardinia, Italy*.

Hanjalić, K., Popovac, M. & Hadžiabdić, M. 2004 A robust near-wall elliptic relaxation eddy-viscosity turbulence model for CFD. *Int. J. Heat Fluid Fl.* **25**, 1047–1051.

Jayatilleke, C.L.V. 1969 The influence of Prandtl number and surface roughness on the resistance of the laminar sub-layer to momentum and heat transfer. *Prog. Heat Mass Transfer* **1**, 193–329.

Manceau, R. & Hanjalić, K. 2002 Elliptic Blending Model: A New Near-Wall Reynolds-Stress Turbulence Closure. *Phys. Fluids* **14** (2), 744–754.

Manceau, R., Perrin, R., Hadžiabdić, M., Fourment, P. & Benhamadouche, S. 2009 Turbulent jet impinging onto a rotating disc: A collaborative evaluation of RANS models. In *Proc. 6th Int. Symp. Turbulence, Heat and Mass Transfer, Roma, Italy*.

Menter, F. R. 1994 Two-equation eddy-viscosity turbulence models for engineering applications. *AIAA J.* **32** (8), 1598–1605.

Minagawa, Y. & Obi, S. 2004 Development of turbulent impinging jet on a rotating disk. *Int. J. Heat Fluid Fl.* **25**, 759–766.

Ničeno, B. & Hanjalić, K. 2004 *Modeling and Simulation of Turbulent Heat Transfer*, chap. Unstructured large-eddy- and conjugate heat transfer simulations of wall-bounded flows. WIT Press.

Popiel, C.O. & Boguslawski, L. 1986 Local heat transfer from a rotating disk in an impinging round jet. *J. Heat Transf.* **108**, 357–364.

Steiner, H., Jakirlić, S., Kadavelil, G., Manceau, R., Sarić, S. & Brenn, G. 2009 13th ERCOFTAC workshop on refined turbulence modelling, 25–26th September, 2008, Graz university of technology, Austria. *ERCOFTAC Bulletin 79* .

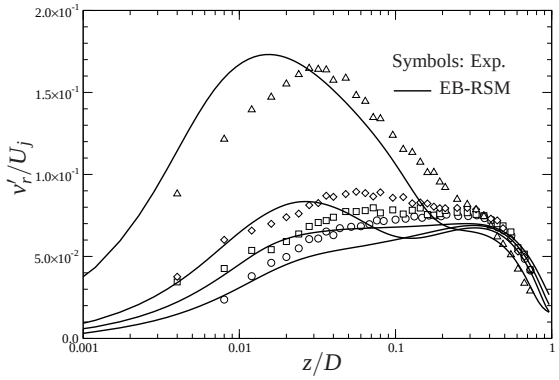

Figure 7. Influence of rotation on the radial rms velocity at the edge of the disk.

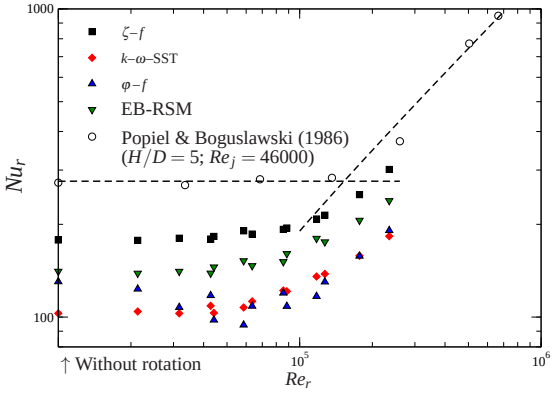

Figure 8. Nusselt number $Nu_r = hr/\lambda$ as a function of Re_r.

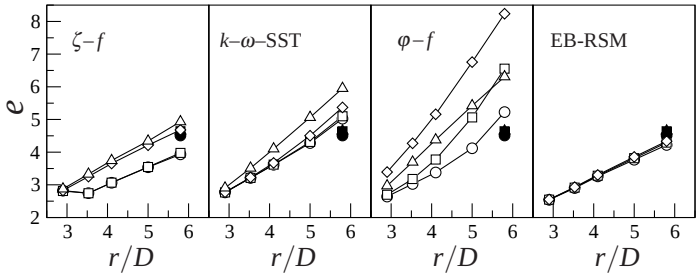

Figure 9. Radial evolution of entrainment ratio e for $\omega D/U_j = 0.00$ (○); 0.12 (□); 0.24 (△); 0.48 (◇). Filled symbols: Experiments.

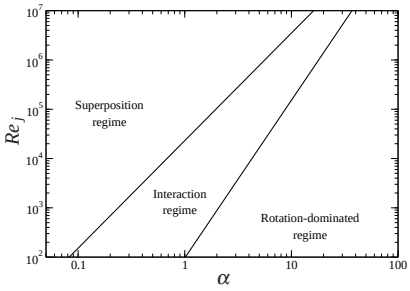

Figure 10. Different regimes in the plane α–Re_j.

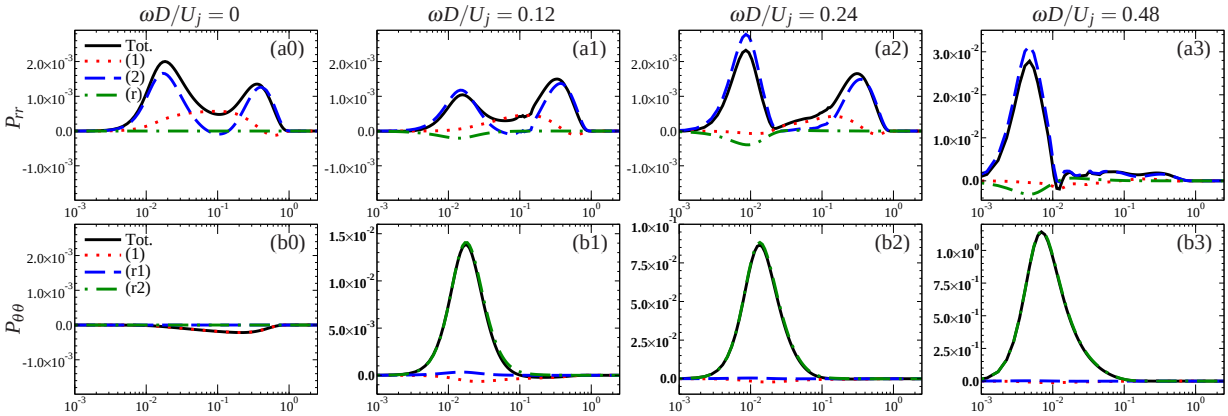

Figure 11. Contributions to production at the edge of the disk for the four rotation rates (EB-RSM computations), made non-dimensional by U_j and D.

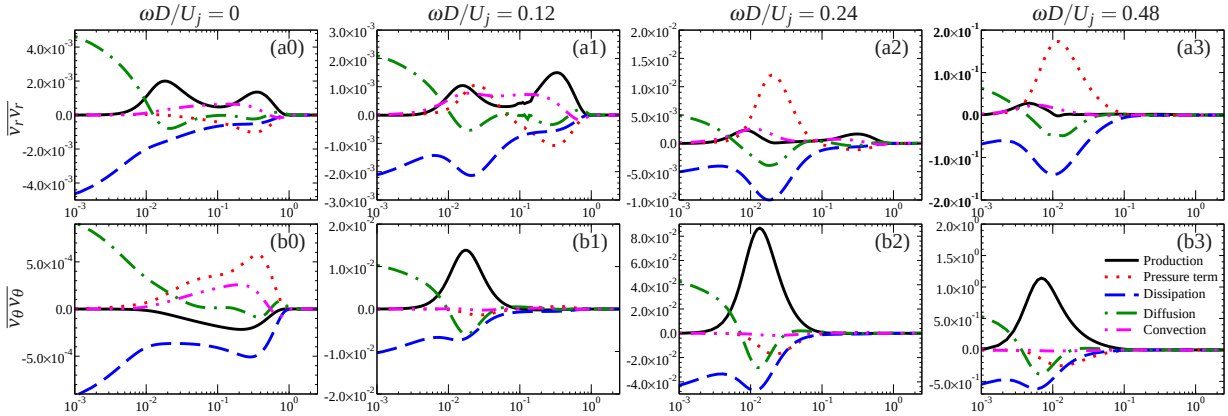

Figure 12. Budgets of the Reynolds stresses at the edge of the disk for the four rotation rates (EB-RSM computations), made non-dimensional by U_j and D. The legend is in the plot (b3).